Adv. Manuf. (2017) 5:20–34
DOI 10.1007/s40436-016-0155-4

Nano-machining of materials: understanding the process through molecular dynamics simulation

Dan-Dan Cui[1] · **Liang-Chi Zhang**[1]

Received: 7 July 2016 / Accepted: 6 September 2016 / Published online: 27 September 2016

Abstract Molecular dynamics (MD) simulation has been widely applied in various complex, dynamic processes at atomistic scale, because an MD simulation can provide some deformation details of materials in nano-processing and thus help to investigate the critical and important issues which cannot be fully revealed by experiments. Extensive research with the aid of MD simulation has provided insights for the development of nanotechnology. This paper reviews the fundamentals of nano-machining from the aspect of material structural effects, such as single crystalline, polycrystalline and amorphous materials. The classic MD simulations of nano-indentation and nano-cutting which have aimed to investigate the machining mechanism are discussed with respect to the effects of tool geometry, material properties and machining parameters. On nano-milling, the discussion focuses on the understanding of the grooving quality in relation to milling conditions.

Keywords Molecular dynamics · Nano-milling · Nano-indentation · Nano-cutting · Groove quality · Multi-grooving

1 Introduction

Ultra-precision and complex miniaturised devices or components with nano-scale surface features are in growing demand with the rapid development of many industries, such as medicine, optics, telecommunication, military and aerospace [1]. These devices or components usually possess good portability and disposability, high purity and interfacial effects, lower material and power consumption, higher heat transferability, and better process integration and automation [2]. However, their manufacture requires repeatable and reliable fabrication methods, high accuracy, precision features and elaborate process design. Nano-machining has been identified to be able to meet the requirement above due to its prominent advantages, such as its high flexibility and precision. In many nano-machining processes, concurrent to the tool feeding ahead and/or rotating, a series of intriguing physical phenomena usually take place in workpiece materials, such as phase transformation and dislocation nucleation. Since nano-indentation is a simple technique for the investigation of mechanical properties on small volumes of materials and is able to capture the above-mentioned phenomena, it has been widely used to understand the fundamental issues related to various nano-machining processes.

At the nano-scale, many important issues cannot be directly revealed by experimental means. Thus MD analysis as a powerful numerical tool has been widely used to provide some deformation details of workpiece materials in the development of nano-machining processes. An MD simulation allows for an in-depth understanding and interpretation of valuable physical phenomena. For example, MD simulations have been applied in probing the micro-/nano-metric behaviour of materials, such as phase transformation, dislocation propagation and stress distribution caused by tool-work interactions.

The objective of this paper is to review some fundamentals with respect to the application of MD simulations in the investigation of nano-cutting and nano-milling.

✉ Liang-Chi Zhang
liangchi.zhang@unsw.edu.au

[1] Laboratory for Precision and Nano Processing Technologies, School of Mechanical and Manufacturing Engineering, The University of New South Wales, Sydney, NSW 2052, Australia

Nano-indentation will be first discussed as this can facilitate basic understanding of MD and nano-machining.

2 Nano-indentation

2.1 Single crystalline

There are extensive works done on MD simulations of nano-indentation on single crystalline materials, such as on silicon which is brittle and on aluminium which is ductile. For example, Zhang and Tanaka investigated the nano-indentation of single crystalline silicon based on MD analysis and clarified a number of fundamental issues in nano-scale investigations, such as stress determination, atomic scale contact area calculation and temperature conversion [3]. Their study showed that octahedral shear stress played a key role in phase transformation from diamond to amorphous structures, while the hydrostatic stress altered the threshold of the phase transformation. They also found that due to the anisotropy of the silicon structure, the critical stresses for initiating inelastic deformation in different directions were different. They reported that such threshold values of the octahedral shear stresses were 4.6 GPa and 7.6 GPa in directions [100] and [110], respectively. Cheong and Zhang revealed that diamond cubic silicon transformed into β-silicon upon loading of indentation process, as shown in Fig. 1 [4]. They also found that the body-centred tetragonal silicon transformed to amorphous phase during unloading and this transition was reversible by conducting the second indentation. To investigate the material behaviour under wet conditions, Tang and Zhang [5] studied a nano-indentation process with a water layer between the silicon substrate and diamond indenter, and found that the presence of water led to the formation of more β-silicon under the same level of external load as in the dry indentation.

Kim and Oh [6] carried out similar MD simulations of nano-indentation on the (100) and (111) surfaces of single crystal silicon along the [100] and [111] directions. They found the phase transformation related to the slip systems in the material. Sixfold and fourfold coordinated structures appeared when silicon was loaded in the [100] and [111] directions, respectively, as shown in Fig. 2. Their study also confirmed the findings by Zhang and Tanaka [3] that both deviatoric and hydrostatic stresses played an important role.

2.2 Polycrystalline

Many engineering applications use polycrystalline materials. It is important to study how the structures yield compared with single crystal structures under the same indentation condition. Minor, Asif, Shan, Stach, Cyrankowski, Wyrobek and Warren conducted the MD simulation of nano-indentation on polycrystalline aluminium to understand the onset of plasticity [7]. The study claimed that plasticity in a dislocation-free volume of polycrystalline aluminium could begin at a very small force, even before the first sustained rise in repulsive force. A submicrometre grain of aluminium could be plastically deformed by nano-indentation to a dislocation density of 10^{14} m^{-2}, making the material reach a shear stress close to its theoretical shear strength. This is inconsistent with the assumption that a dislocation-free volume is necessary

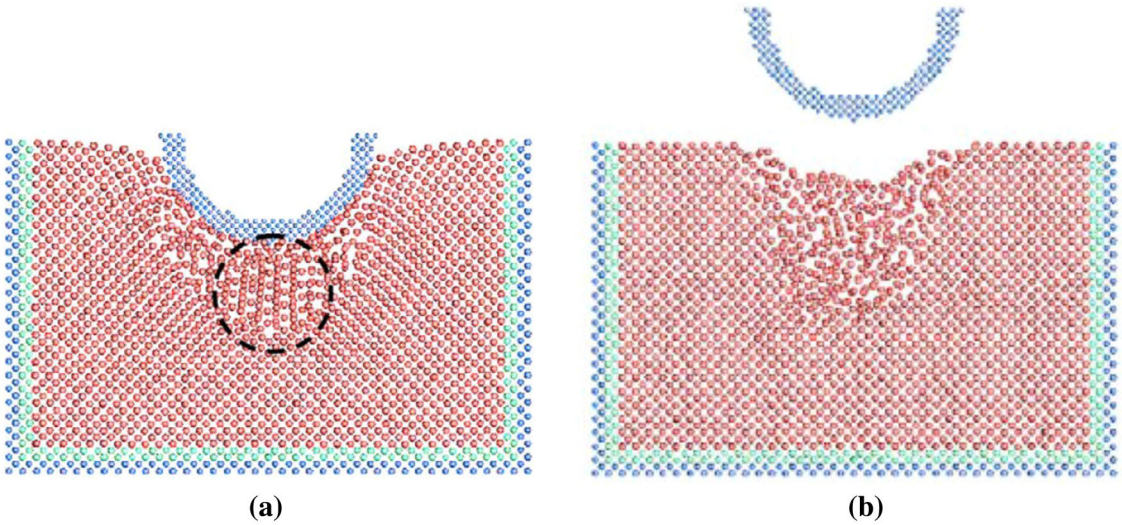

Fig. 1 Silicon phase transformation: **a** at maximum indentation, atoms beneath the indenter (*circled by the dotted line*) have a crystalline order different from that of the original diamond cubic structure; **b** crystalline to amorphous transition upon unloading [4]

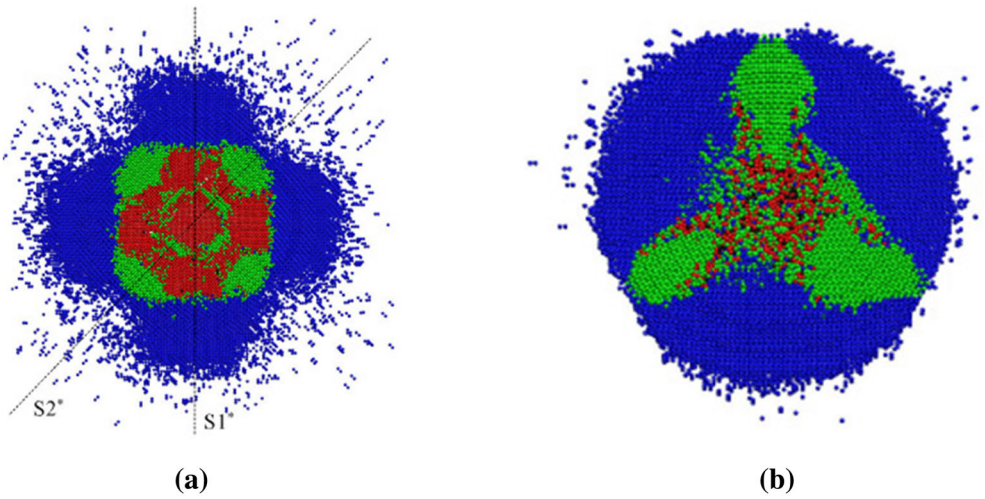

Fig. 2 Effect of crystal anisotropy on phase transformation in nano-indentation on **a** Si (100) surface and **b** Si (111) surface [6]

to achieve shear stresses near the theoretical shear strength of the material.

An MD simulation of nano-indentation has also been performed to investigate the dislocation interactions with a grain boundary [8]. A nickel bicrystal with a vertical $\Sigma = 5$ (210) grain boundary was indented by a diamond indenter, where Σ was the degree of fit between the structures of two grains. The results suggested that propagating dislocation loops merged into the grain boundary leading to the migration of the lateral grain boundary. An analysis of the atom movement during the indentation showed that the grain boundary migration was caused by the interactions of the lattice dislocations with grain boundary dislocations, resulting in cooperative atom motions near the grain boundary.

Nano-indentation of polycrystalline copper has been carried out with the aid of MD simulation as well [9]. The hardness, elastic recovery ratio and temperature of polycrystalline copper were found to strongly depend on crystal structure and twin-lamellae-thickness. It was seen that initial dislocation always nucleated at the beneath of indenter, and bursted during the indentation process. Moreover, the plastic deformation of the polycrystalline copper depended on the dislocation–grain boundary (GB) interactions.

2.3 Amorphous material

An MD study of nano-indentation of amorphous silicon carbide was performed and a correlation between the atomic structure and the load-displacement (P-h) curve was obtained [10]. The short range of P-h responses of α-SiC showed a series of load dropped associated with the local rearrangements of atoms, similar to that of crystalline 3C-SiC. Nevertheless, the load drops were less pronounced and nano-indentation damage was less localized. The onset of plastic deformation took place at the depth of 0.05 nm, which was around one quarter of the corresponding value in 3C-SiC.

The behaviour of amorphous alloy Cu50Zr50 was also studied with the aid of MD simulations [11]. It is found that shear transformation zones constantly migrated and growed during the indentation process. A bigger indentation depth, loading speed and indenter radius led to a larger loading force. The increase of loading speed results in an increase of the material's hardness and elastic modulus, but the change of indenter radius was found to have a negligible effect. Increasing the machining temperature was accompanied with the decrease of load and hardness but increased in the elastic modulus.

The understanding towards the theory of nano-indentation measurements has improved in recent years. However, many questions remain. For example, even though experiments show that the geometry of indenters plays a key role in nano-indention, little work has been done using MD simulations [12, 13]. The deformation of many materials is highly strain rate dependent, but little has been performed.

3 Nano-cutting

Scaling down from the macro-scale to the micro-/nano-scale has created numerous challenges. There is a wealth of literature about MD simulations of nano-cutting and impressive progress has been made. For instance, Cheong et al. [14], and Zhang and Cheong [15] described in detail the essentials of MD simulations for nano-cutting, such as the control volume determination, boundary condition setup, time step justification and potential function selection. Cheong and Zhang [16] investigated the effect of

multiple cutting tips on the damage mechanisms of nano-cutting. Zhang et al. [17] explored the possibility of reaching the theoretical shear strength of tool-workpiece friction when the depth of cut was critically small. Since many simulation fundamentals have already been well documented in relation to nano-cutting, this section will merely focus on the effects of some key cutting parameters on the subsurface damage, such as tool geometry, material properties and machining parameters.

3.1 Tool

At the nano-scale, questions were proposed regarding if the tool influenced the machining process in the same way as at the macro- and micro-scales, which had instigated much literature.

3.1.1 Tool materials

Unlike macro-/micro-machining, the plastic deformation at a nano-scale process is very small. As such the hardness of a tool is often greater than that of the workpiece material. A systematic MD simulation of the nano-sliding process successfully correlated the tool material properties to the dynamics wear of tools [18]. In the study, a variety of "infinite" hard materials, such as diamond, tungsten, chromium and iron, were selected as the tool materials. The simulation results proved that with a decrease in the tool hardness, tool wear became severer and chipping was less efficient.

3.1.2 Rake angle

The rake angle, which played a key role in machining at the macro- and micro-scale, was analysed at the nano-scale as well. In nano-machining, the edge of the cutting tool is not perfectly sharp compared with the shallow cutting depth which can be as small as a few angstroms. The blunt edge and effective rake angle may result in different machining mechanisms, such as the subsurface deformation and chip formation. Therefore, study on tool features, such as rake angle, becomes non-trivial. Numerous MD studies of different nano-machining processes have uncovered the effects of tool rake angle on the chip formation mechanism [19, 20] and the resultant cutting forces [21, 22]. For example, through nano-cutting simulations on copper by extremely sharp and infinitely hard tools with different negative rake angles (0°–75°) [20], it was observed that the increase of the negative rake angle resulted in a decrease in chip length but an increase in ploughing ahead of the tool and subsurface deformation underneath the machined surface. The smaller chip is attributed to the larger plastic deformation generated in the workpiece [19] (see Fig. 3), while the plastic deformation occurred in front of the cutting tool tip, and was due to the hydrostatic pressure under the negative rake angle [23]. The variation of the rake angle was also found to lead to the oscillation of cutting forces in nano-cutting. For instance, with the rake angle changing from $+10°$ to $-75°$ the thrust force rose sharply [20]. To reveal the underlying physical meaning, an MD study of dry polishing with a variation of rake angles was carried out [21]. It was found that when the rake angle was negative, the horizontal cutting force increased with the decrease of the thrust force, which resulted in less compression but an enhanced cutting effect. In contrast, when the tool rake angle was in the range of 0°–20°, the cutting force increased with increasing the rake angle.

3.1.3 Clearance angle

The clearance angle effect on nano-cutting has also been studied. The partial elastic recovery was found to occur under the clearance face in the micro-machining procedure, which caused a mass of ploughing and tool wear. Through a group of nano-cutting tests on silicon with different clearance angles [24], the change of clearance angle was found to bring about different degrees of compaction of the machined surface beneath the cutting tool but no subsurface deformation. The above observation seems to indicate that subsurface deformation is closely related to the compression of the material underneath the tool. Through the nano-cutting on copper with the aid of MD simulations, the influence of clearance angle on the cutting force and surface finish was analysed [25]. The approximate entropy and stress distribution, representing the complexity and uncontrollability of the cutting force, revealed that the reduction of the clearance angle resulted in a worse surface finish but a stable and controllable cutting force.

3.1.4 Tool cutting edge radius

At the nano-scale, the dimension of tool radius is comparable with the depth of cut, such that it is essential to investigate the combined effect of these two parameters to the machining process. Nano-cutting investigations have been conducted with the aid of MD simulations by varying the tool edge radius (3.62–21.72 nm) and depths of cut (0.362–2.172 nm) while maintaining the ratio of the depth of cut (d) to the tool edge radius (r) constant at 0.1, 0.2 and 0.3 [22]. The number of dislocations was found to rise with the increase of depth of cut at a given ratio. This is attributed to the increase of cutting forces in the process. In contrast, the subsurface deformation increases with decreasing the ratio d/r. However, this study did not involve the investigation of chip formation. Later on, an MD simulation of nano-cutting on single crystal silicon

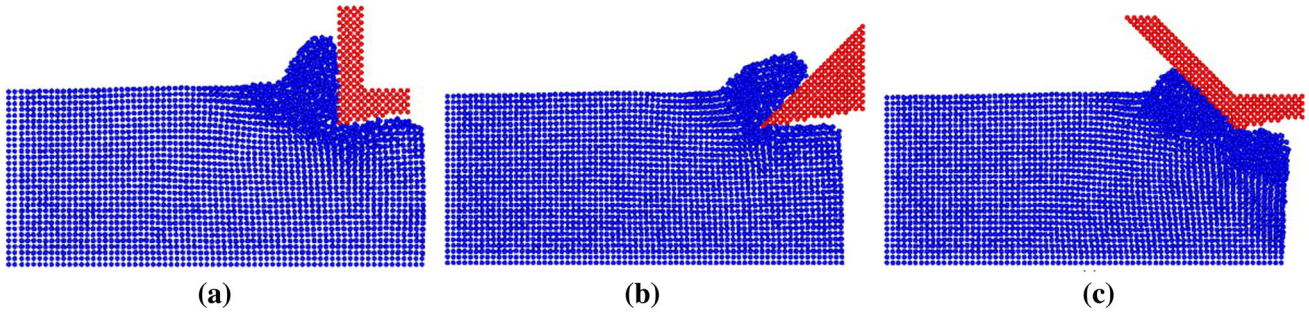

Fig. 3 Snapshots of the nano-cutting process with the tool rake angle **a** 0°, **b** 45° and **c** 45° [19]

was carried out [26]. Similar to the conclusions made by Zhang and Tanaka [27] on the nano-cutting of copper and Zhang and Tanaka [28] on the nano-cutting on silicon, it was found that when the ratio was less than a critical value, the chip formed through extrusion. When this ratio exceeds a threshold value, however, chip formation occurs via a brittle mode.

The cutting edge radius also has an impact on cutting forces. Some studies have claimed that the ratio of the thrust force to the cutting force remains unchanged at a lower edge radius [29], but that it increases with the increase of the edge radius. At a smaller tool radius, an increase of cutting edge radius leads to an increase in the cutting forces, but these forces become independent of the edge radius at higher values of tool edge radius.

3.2 Workpiece material

The effects of the anisotropic behaviour (single crystalline materials) [30] and grain boundaries (polycrystalline materials) play a vital role in the nano-machining of crystalline materials [31].

3.2.1 Single crystalline

In nano-machining, the crystal orientation and cutting direction have strong effects on the subsurface deformation of the work material, dislocation movement and cutting forces. An MD simulation of nano-cutting of single crystal aluminium with different crystal orientations and cutting directions [30] showed that the plastic deformation ahead of the tool was accomplished predominantly by compression along with shear in the cutting direction when the crystal was orientated in (111) plane and cut in the direction. With the progress of cutting, deformation occurred in the material in the zone ahead of the tool, and in the region several layers below the tool tip. In the case of (001) orientation and [100] cutting direction, dislocations were parallel to the cutting direction. Nevertheless, when the cutting was in the [001] direction and the crystal was orientated in (110) plane, dislocations became normal to the cutting direction. However, when the crystal orientation was in (110) but cut in $[\bar{1}10]$, dislocations occurred both along and normal to the cutting direction. Subsurface deformation varied with different orientations of the crystal and cutting directions. No dislocation was observed within the subsurface parallel to the cutting direction, and the dislocations generated perpendicular to the cutting direction moved towards the machined surface due to elastic recovery.

An MD simulation was also conducted to identify the influence of crystal orientation on deformation characteristics by scratching a single crystal silicon (100) surface with a hemispherical diamond tip of radius 7.5 nm along [100] and [110] directions [32]. At a relative large depth of cut (1 nm and 1.5 nm), a body-centred-tetragonal (BCT-5) silicon layer of around 1 nm thickness emerged beneath the amorphous layer when scratching along [110]. When scratching along [100], however, twinning would occur in the subsurface with the absence of the BCT-5 silicon layer.

To investigate the anisotropy effect, MD simulations of nano-indentation and scratching of single crystalline aluminium have been carried out with specific combinations of orientations and scratch surfaces to study the orientation effect on the cutting forces at the nano-scale by Komanduri et al. [33]. It was observed that the minimum normal force was along the (111) orientation, which was consistent with the most favoured slip system for a face-centred cubic (FCC) material. The resultant force during the scratching process was found to be minimum along the (111) $[\bar{1}10]$ orientation and maximum along the (111) $[\bar{2}10]$ orientation, respectively.

An MD nano-cutting study of copper along different directions on different surfaces was performed to correlate the cutting forces with subsurface deformation by Pei et al. [34]. It was found that the lowest cutting force was in the case of (001), while the highest was in the case of (111). This was attributed to the cutting force projection along the dislocation slip directions and the required force to drive the dislocations to generate deformation, because a larger

propagation angle resulted in a higher requirement of the resultant cutting forces.

3.2.2 Polycrystalline

When the grain size was decreased to the nanocrystalline level, the deformation behaviour of the material became critically related to the grain size [35]. A number of MD studies have been carried out to understand the mechanism.

The MD studies on polycrystalline FCC metals [36] showed that grain boundaries in nanocrystalline metals had a short range structure among conventional polycrystalline materials. There is a threshold value below which no intra-grain deformation can be detected and all the plastic deformation is located in the grain boundary.

Some investigations have been conducted to examine the influence of applied force and grain boundary misorientation on grain boundary sliding on two arranged grains [37]. It was found that for any given misorientation, the increase of applied force resulted in three basic behaviours: no sliding, constant velocity sliding and parabolic sliding. The relationship between the constant sliding velocity and the applied stress was linear. In contrast, the parabolic sliding process was accompanied with disordering of atoms along the grain boundary.

The effects of crystallographic orientation have been addressed by MD through the scratching on a nano-twinned copper workpiece (containing embedded twin boundaries parallel, inclined and perpendicular to scratching surfaces with different twin spacing) [38]. This work showed that the random coupling of crystallographic orientation and twin boundary orientation with respect to the scratching direction strongly influenced the competition between individual deformation mechanisms. In turn, this affects the fractional contribution of each deformation mechanism to the overall frictional response and results.

3.3 Machining parameters

Similar to that at the macro-/micro-scale, performance at nano-scale is influenced by machining parameters, including machining velocity and depth of cut.

3.3.1 Depth of cut

Zhang and Tanaka [27, 28] carried out systematic studies which provided the fundamental understanding about the machinability in nano-cutting on copper and silicon and predicted the lower bound of depth of cut for possible material removal. The studies revealed four regimes of deformation, i.e., no-wear regime, which was defect free, adhering regime where surface atom exchange took place, ploughing regime which was characterized by a moving triangular atom-cluster, and cutting regime where material removal occurred. The transitions between these regimes were found to be governed by the sliding/cutting parameters such as depth of cut, cutting speed and cutting edge geometry.

The minimum thickness of cut was defined as the uncut thickness below which material removal could not take place in the form of a chip. The minimum thickness of cut was found to be affected by the tool-workpiece interaction and the sharpness of a cutting edge. A 3D MD simulation of nano-machining has been performed with different depths of cut (0.362–2.172 nm) [22]. The extent of plastic deformation in front of the cutting tool and in the subsurface and the number of dislocations increased when the depth of cut increased. A study from a nano-cutting on a silicon wafer by a diamond tool indicated that with an increased depth of cut, dislocation density increased, associated with a rise in the cutting forces [23]. Crystal deformation and chemical bond fracture could eventually occur.

3.3.2 Machining velocity

In the nano-cutting of single crystalline copper [39], it was noted that when the cutting speed was low, the machined surface was smooth with dislocations inside the workpiece. However, a higher cutting speed would lead to a rather rough surface, but the subsurface of the workpiece became dislocation-free. In addition, with an increased cutting speed, the chip size grew accordingly.

Such cutting speed effect has been investigated with an MD simulations on single crystal copper [34]. It was found that a higher cutting speed led to more defects because the cutting forces increased with the increase of the cutting speed. However, nano-cutting at 50 m/s, 100 m/s, 150 m/s and 200 m/s resulted in essentially a constant cutting force, indicating that the cutting force was not influenced by the cutting velocities [40]. In an MD simulation of AFM-based nano-cutting, different cutting speeds (50 m/s, 100 m/s and 400 m/s) were used [41]. The results showed that a higher cutting velocity resulted in a larger cutting and normal force, due to the larger volume of chips generated in front of the AFM tip. Under a high cutting speed, the dislocations had less time to move away from the cutting zone, and the material piled up in the machining region, to make the cutting forces greater. The larger chip volume also brought about a larger force.

MD simulations of nano-scratching on single crystalline, polycrystalline and nanotwinned (NT) polycrystalline copper have been performed at different scratching velocities to study the plastic deformation mechanisms [42]. It was observed that the increasing scratching rate led to

continuous increase in scratching force and workpiece temperature, and then results in dislocation slip, grain boundary slip, and twinning/detwinning, which is attributed to severe plastic deformation and large chip volume. Scratching rate was also found to govern the distributions of potential energy and kinetic energy of all the atoms, revealing the rate-dependent plastic deformation. In detail, the plastic deformation for different scratching rates depends on the competition of scratching force, workpiece temperature and tool-workpiece contacting time that affect dislocation evolution.

3.4 Multiple grooves

With the increasing demands of intricate structures on ultra-precision components, the stability and profile quality of device structures must be guaranteed. Among these, the fabrication of multiple straight grooves can reveal the machining mechanism, even though this is the most basic and simple process.

Comprehensive MD studies have revealed the machining mechanism of multi-grooving and the influence of machining parameters. For example, in the reciprocating cutting process, atoms are removed mainly by compressing, extruding and attracting because defects from the prior cutting process restrict the movement of dislocations [43]. The surface quality of a nano-machined surface and the shape of the scratched groove were found to have a close relationship to the offset distance of the tool. The affected zone from the second feeding cutting process is larger than that from the prior cutting process. The second feeding cutting force increases as the offset distance of the tool increases.

Cutting force characteristics have also been studied. Simulation results from the nanometric multi-grooving of copper revealed that the average tangential and normal components of the cutting forces increased with increasing the depth of cut [44]. In addition, the two forces decrease at any given depth of cut in the consecutive cutting pass, and the ratio of the tangential force to the normal force decreases with the increase of depth of cut. The ratio of the cutting force to the cutting cross sectional area decreases with an increased depth of cut but remains unchanged when the depth of cut rises to over 2.5 nm.

In brief, the MD technique has contributed a lot in revealing machining mechanisms in nano-cutting. However, there are still critical issues that need to be addressed, some of which are

(i) Comprehensive MD studies have uncovered that tool hardness and tool geometries such as rake angle, clearance angle and cutting edge radius influence tool wear and chip formations. However, the structures of the tools used in MD simulation are mostly simplified, making the simulation inconsistent with the actual situation.

(ii) The effects of material anisotropy and grain boundary have been investigated, showing that subsurface deformation varies with crystal orientations and cutting directions. These models, however, are not applicable to complex crystalline materials. Moreover, a more reliable investigation on residual deformation without the loading of the cutting tool would be useful and should be considered in further MD simulation studies.

(iii) MD simulations offer a good understanding of the effects of machining parameters, including depth of cut and machining velocity. However, controversy still exists regarding the relationship between cutting speed and cutting force. For example, the cutting force was claimed to be independent of the cutting speed, which conflicts with the opinion that a higher cutting speed leads to severer material strengthening and larger cutting forces. A thorough study is therefore necessary to clarify the correlations between the cutting force and cutting speed.

(iv) MD simulations have explored the machining mechanism of multi-grooving. Even though the second feeding cutting force is found to correlate with the offset distance of the tool, the causes have not yet been analysed and the minimum distance between the adjacent grooves guaranteeing multi-groove qualities has not been identified. The influence of many machining parameters, for instance the cutting speed, has not been considered. Moreover, apart from the sequential cutting method, simultaneous multi-grooving has not yet been investigated.

4 Nano-milling

In this section, the work about MD simulation of nano-milling will be discussed, including both single-grooving and multi-grooving.

4.1 Single-grooving

MD simulation of single-groove nano-end-milling on single crystal copper martial with a rigid diamond tool was performed to investigate the nano-machining mechanism by Cui et al. [45, 46]. The nano-milling operations were carried out along the $[\bar{1}00]$ direction on the (001) surface of the workpiece, as shown in Fig. 4. When the milling tool fed in at feed rate f, it also rotated at rotational speed n anticlockwise.

4.1.1 Milling force

The milling force was investigated by analysing milling pattern and comparing with the analytical force model which was developed for the micro-scale [45]. The variations of the feeding force F_x and traverse force F_y in a nano-milling process were captured and shown in Fig. 5a, with a clear visualization of the forces within a single tool revolution enlarged in Fig. 5b. It was found that the time between homologous points on every other peak corresponded to each pass of the milling edge with reference to the rotational speed of the tool.

Besides, the feeding and traverse forces were found to follow a sinusoidal path and semi-sinusoidal path, respectively [47]. Such force variation patterns were explained by the analysis of the nano-milling process, as shown in Fig. 6. It was seen that only one cutting-edge of the milling tool was in contact with the workpiece in the upper half (shaded region) of the tool path. As the tool rotated, the cutting edge would move from the first quadrant to the second, leading to a positive feeding force in the first quadrant and a negative force in the second quadrant. Thus the traverse force was always positive.

It was also found the periodic force variation shown in Fig. 5 had a good agreement with that in micro-/macro-milling [48]. The analytical tangential force model for the micro-end-milling [48] was still considered suitable for studying nano-channel fabrication by Wang et al. [49], so it was expected that the analytical force model Eq. (1) which was developed for the micro-end-milling could be used to predict the nano-milling force,

$$F_t = K_m A_c, \tag{1}$$

where F_t is the tangential cutting force, K_m is material coefficient and A_c is atomic contact area. Since single crystal copper is anisotropic, which accounts for the main difference between the micro-/nano-scale and macro-scale and plays a very important role in the nano-scale, the orientation effect leads to the different material properties along different directions. Thus a quarter of a nano-milling revolution was divided into small cutting steps with continuously varying directions. The material coefficients K_m along different directions—including $[\bar{1}00]$, $[\bar{5}\,\bar{1}0]$, $[\bar{5}\,\bar{2}0]$, $[\bar{2}\,\bar{1}0]$, $[\bar{1}\,\bar{1}0]$, $[\bar{4}\,\bar{7}0]$, $[\bar{2}\,\bar{5}0]$ and $[\bar{2}\,\bar{7}0]$—on (001) surface were then calculated by performing separate cutting simulations along those directions. As shown in Fig. 7, the variation of K_m with the cutting directions which were translated into azimuthal angles, in which K_m reached its peak value at 45°. This pattern was found to be similar to the simulation results above. The contact area between the indenter and workpiece was calculated by counting the number of C-Cu atom pairs and adding those atomic contact areas [50] as expressed as follows

$$A_c = \pi r_a^2 N_c. \tag{2}$$

Thus the analytical milling forces at different azimuthal angles within a single tool revolution was calculated and then compared with those from MD simulation, as shown in Fig. 8. They were found to be in very good agreement. Therefore, it is clear that a nano-milling MD simulation, performed with rationalized parameters, can further explore the nuances of the nano-milling process, and provide reliable and insightful information for nano-machining analysis.

4.1.2 Groove profile

A set of criteria was developed to evaluate groove profile quality, following which the groove profiles for different

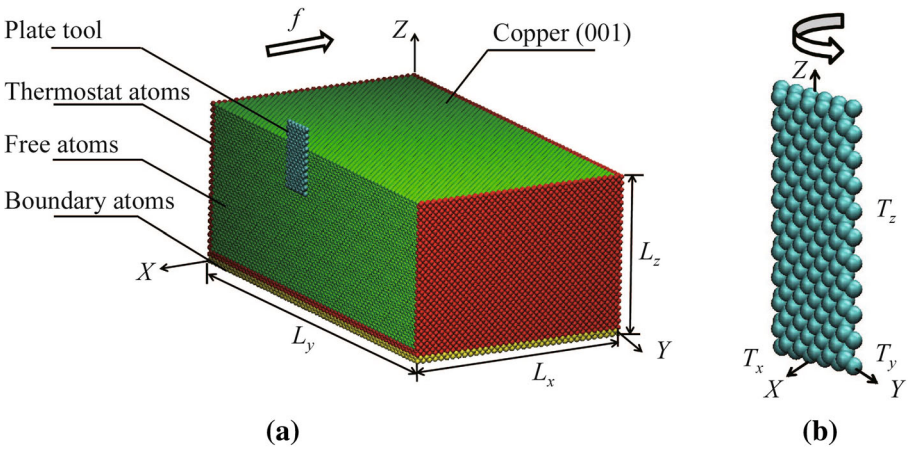

Fig. 4 **a** The control volume of the single crystalline copper workpiece, where *red dots* are thermostat atoms, *yellow dots* are fixed boundary layers and *green dots* are Newtonian atoms and **b** milling tool [45]

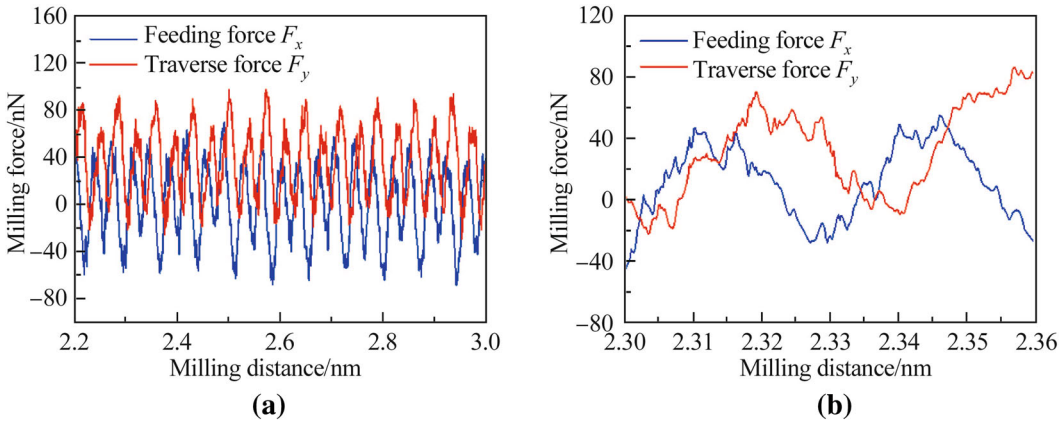

Fig. 5 **a** Variations of the feeding force F_x and traverse force F_y in nano-milling and **b** enlarged view of the milling forces in a machining cycle [45]

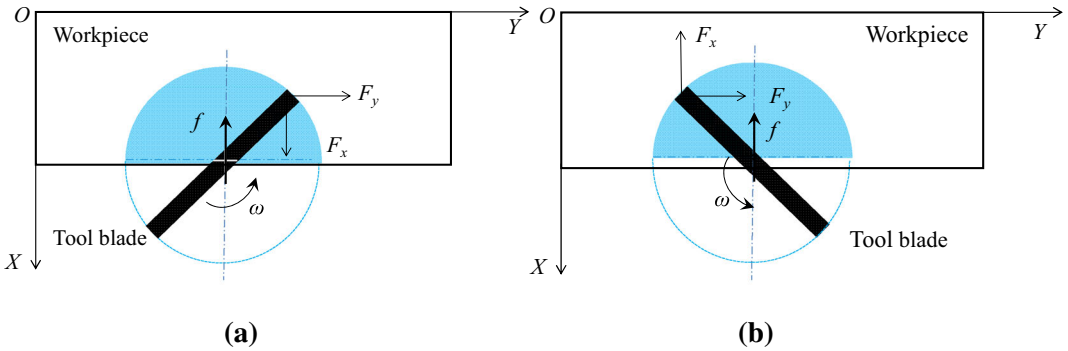

Fig. 6 Tool path and force direction in a milling process (*top view*). **a** the cutting blade in the zone with increasing thickness of cut and **b** the cutting blade in the zone with decreasing thickness of cut [47]

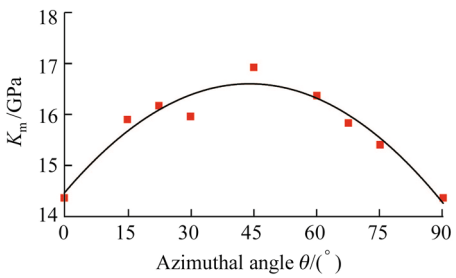

Fig. 7 K_m versus azimuthal angle of single crystal copper [45]

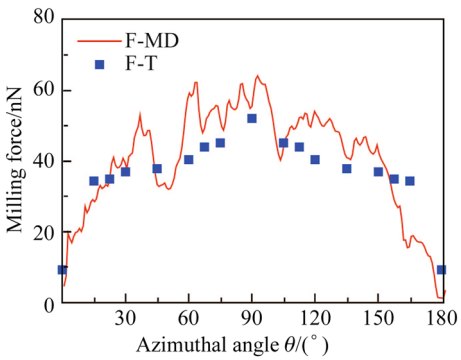

Fig. 8 Theoretical (*blue diamonds*) and MD simulation (*red curve*) milling tangential forces [45]

nano-milling cases were assessed. Three cases were chosen as examples and shown in Fig. 9. It was summarised that (i) top edges distorted in all the studied cases, (ii) the groove profiled at the outlet side of the tool rotation aligned more closely with the designed geometry, and (iii) increasing depth of cut improved groove quality. To explain the observed phenomena, the key physics parameters, i.e., surface energy, strain rate and residual stress were investigated.

4.1.2.1 Surface energy Since surface energy plays an important role at the nano-scale, it is studied to thoroughly understand the groove formation mechanism. To demonstrate the effect of surface energy, four different positions on the top of workpiece were chosen and analysed, as shown in Fig. 10a. The surface energy at positions A (at the corner), B (at the top edge) and C (on the surface) was 3/4Ψ, 7/12Ψ, and 1/3Ψ (Ψ denoted the binding energy of an atom within a perfect workpiece, as shown in Fig. 10b), respectively. As such, the atoms near the groove top edges

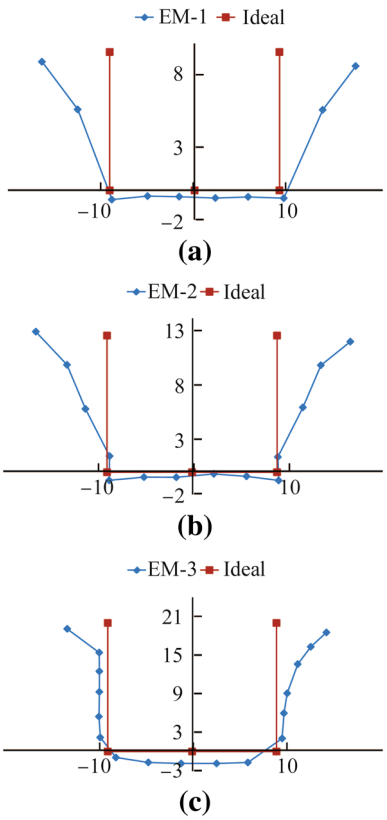

Fig. 9 Variation of average groove profiles with the depth of cut of **a** 0.9 nm, **b** 1.35 nm and **c** 1.8 nm [45]

were unstable, bringing about a distortion. At D (at the bottom edge), the atom had eleven bonds (surface energy is only 1/12Ψ), thus the radius of curvature at the bottom corner was small. This was in good agreement with the characteristics of groove profiles shown in Fig. 9, where the atoms at the top edges of the grooves displaced away, the edge profile got better at a larger depth of cut of 1.35 nm compared with that of 0.9 nm. Sharper top groove edges and straight walls were achieved at the depth of cut of 1.8 nm.

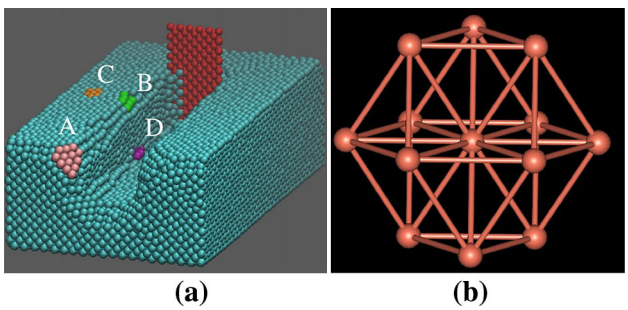

Fig. 10 **a** Surface energy characteristics at different positions of groove, **b** twelve coordinated atom within a perfect copper workpiece [45]

4.1.2.2 Stain rate Strain rate variation during nano-milling was calculated, because the deformation of single crystal copper was highly strain rate dependent material and the distortion of a groove top edge was influenced by the atomic strain rate. The distribution around a single groove for the end milling simulation was shown in Fig. 11. It was observed that the atoms located in the first four atomic layers on each side along the groove had high shear strain rates. In addition, with the tool rotating from 0° to 180°, the atoms ahead of the tool tip always showed high shear strain rates, and extended to about farther. This was to be due to the hard push by the tool tip, which caused a fast atomic flow and then a severe disturbance ahead, resulting in a larger area with high strain rates.

4.1.2.3 Residual stress To understand the deformation of a workpiece during the milling process, residual stress along the length and width of the groove was investigated and shown in Fig. 12 [45]. It was seen that the area with high residual stress near the entrance side was obviously larger than that of the exit side. This was related to the difference of atomic flow at each side. Specifically, when the tool penetrated the workpiece, the atoms in front of the tool were pushed to move ahead accordingly. However, due to the strong elastic constraint from the frontal neighbours, these atoms could only be compressed, leading to an even higher density environment. In contrast, at the exit side, atoms accumulated ahead of the milling tool and could flow outwards easily due to less or even no elastic constraints.

4.2 Mid-wall thickness for multi-grooving

For a systemic study, five different machining methods were carried out, including both sequential and simultaneous methods with the same and opposite rotational directions. In a multi-grooving procedure, mid-wall thickness u was also found to play a key role on multi-groove forming and thus the influential factor of minimum mid-wall thickness was investigated. Based the proposed effective groove quality assessment criteria, the required minimum mid-wall thicknesses $u_{\min}$ for each machining method under different depth of cut d were obtained and summarized in Fig. 13.

It was found that minimum mid-wall thicknesses $u_{\min}$ increased with the increase of depth of cut d and the requirement of $u_{\min}$ to achieve uniform mid-walls in simultaneous grooving (Methods D and E) was higher than the sequential grooving process (Methods A, B and C). To identify the critical value for different methods, sophisticated studies were carried out on the residual shear stress and shear strain rate.

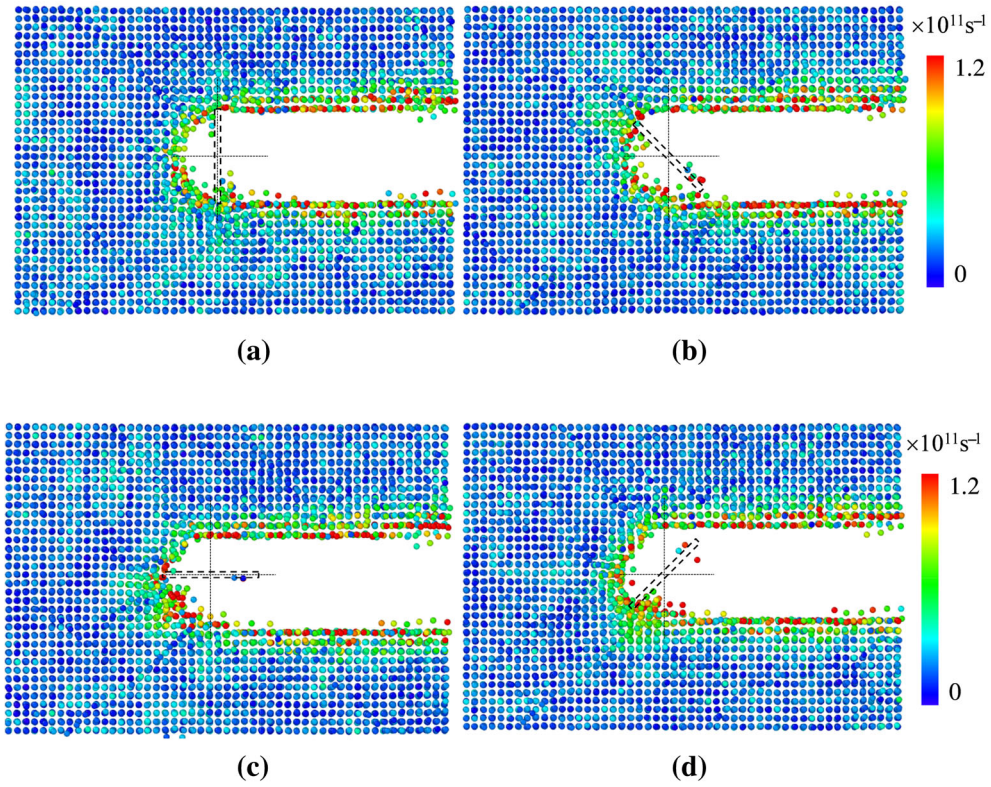

Fig. 11 Strain rate distribution along the groove with the tool's rotational angle at **a** 0°, **b** 45°, **c** 90° and **d** 135° from the *top view* [45]

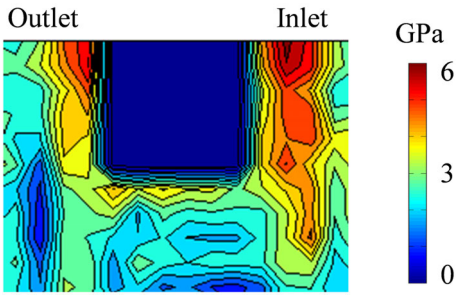

Fig. 12 Residual stress distribution around the groove [45]

4.2.1 Residual stress

The high residual stress distribution (a) around single-groove, in the mid-wall of multi-grooves (b) by Method-A, (c) Method-D and (d) Method-E were studied and shown in Fig. 14. The width of the high residual stress area by the tool's entrance side of groove was around 3*a*, as shown in Fig. 14a. After milling the second groove next to it on the left hand side (by Method-A), the high stress area covered around 8*a* along groove width inside the mid-wall due to the dramatic release of high residual stress on the right hand side of the first groove, as illustrated in Fig. 14b. In both of the simultaneous machining processes, the stress distributions occupied 8*a*, as shown in Figs. 14c, d respectively.

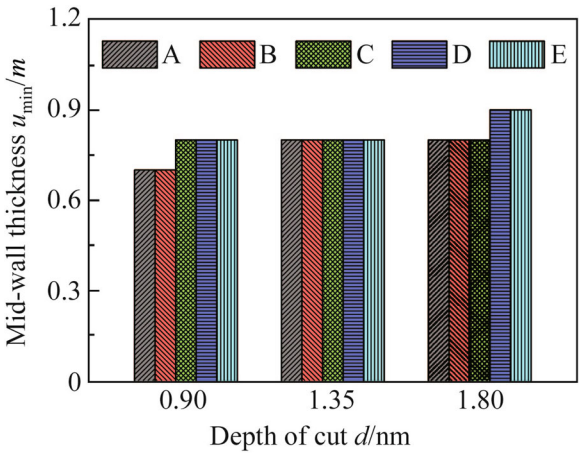

Fig. 13 Minimum mid-wall thickness u_{min} for multi-grooving

4.2.2 Strain rate

The distributions of shear strain rate along groove(s) of the above simulation cases were investigated as well and illustrated from the top view, as shown in Fig. 15. Around the single groove, the atoms with high shear strain rates occupied 2*a* along the groove width direction. Once another groove was fabricated next to the previous one, the high-strain rate distribution covers 3*a* as shown in Fig. 15b.

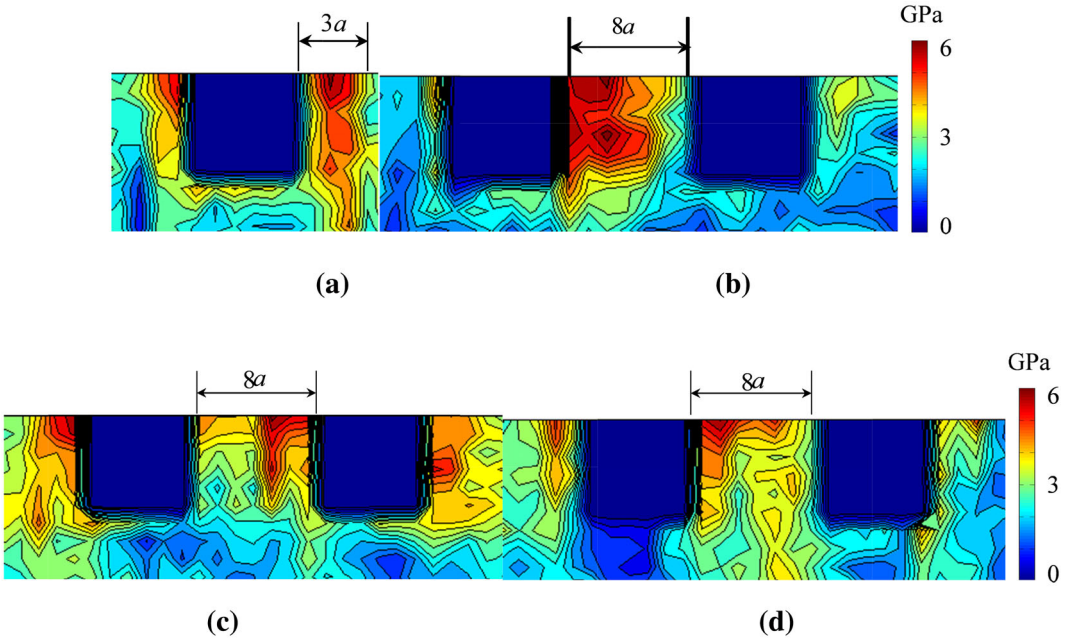

Fig. 14 Stress distribution **a** around single-groove, and in the mid-wall of multi-grooves **b** by Method-A, **c** Method-D and **d** Method-E

In the simultaneous milling process by Method-E, atoms with high-strain rates fully covered the mid-wall (8*a*). It was attributed to that when the two tools approached each other, a cluster of high-strain-rate atoms were pushed ahead by each tool and moved towards the middle layer of the mid-wall. Due to being subjected to symmetric constraints from the two blades, these atoms possessed high potential energy. When the tools departed the mid-wall, these atoms moved energetically to their equilibrium positions, causing a large high shear strain rate area, as shown in Fig. 15c. In contrast, by Method-D, the tools were always parallel with each other and then the strain rates nearby each tool were independent. As such the strain rate distribution patterns along the groove length were the same as that of a single groove, and shown in Fig. 15d.

The strain rate and residual shear stress distribution were found to show good agreement with the required minimum mid-wall thickness for Method-E, and sequential grooving process and Method-D respectively. The analysis of strain rate and residual stress could provide a guidance to the selection of mid-wall thickness parameters for the multi-groove milling.

4.3 Dimensional analysis

Since the groove profile quality by nano-milling was claimed to be affected by both machining parameters and material properties [45, 47], the governing factors were identified to effectively improve the groove quality by carrying out dimensional analysis with the aid of multi-

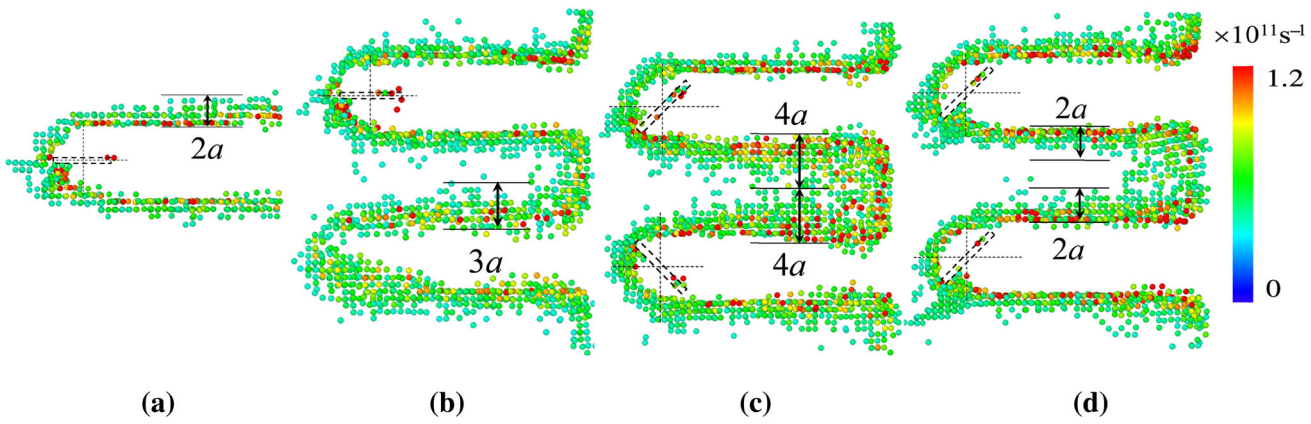

Fig. 15 Strain rate distribution along **a** a single-groove, **b** multi-grooves machined by **b** Method-B, **c** Method-E and **d** Method-D

Table 1 Predictive functions and statistical factor R^2 for all simulation methods

Method	Predictive function	R^2	Eq.
Single	$\frac{AAd}{w} = 0.005\left(\frac{f}{\pi nw}\right)^{0.458}\left(\frac{d}{w}\right)^{-0.263}\left(\frac{n\mu}{\sigma_T}\right)^{0.214}$	0.908	(3)
Method-A	$\frac{AAd}{d} = -1.788\left(\frac{d}{w}\right)^{-1.792}\left(\frac{u}{d}\right)^{-0.567}$	0.991	(4)
Method-B	$\frac{AAd}{d} = -1.815\left(\frac{d}{w}\right)^{-1.773}\left(\frac{u}{d}\right)^{-0.477}$	0.992	(5)
Method-C	$\frac{AAd}{d} = -1.704\left(\frac{d}{w}\right)^{-1.957}\left(\frac{u}{d}\right)^{-0.594}$	0.990	(6)
Method-D	$\frac{AAd}{d} = -1.765\left(\frac{d}{w}\right)^{-1.991}\left(\frac{u}{d}\right)^{-0.604}$	0.993	(7)
Method-E	$\frac{AAd}{d} = -1.763\left(\frac{d}{w}\right)^{-2.084}\left(\frac{u}{d}\right)^{-0.750}$	0.990	(8)

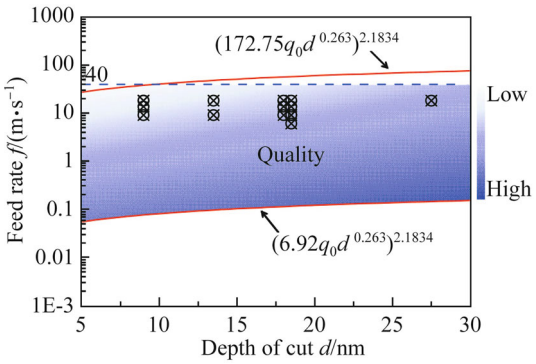

Fig. 16 Machining chart for single-grooving

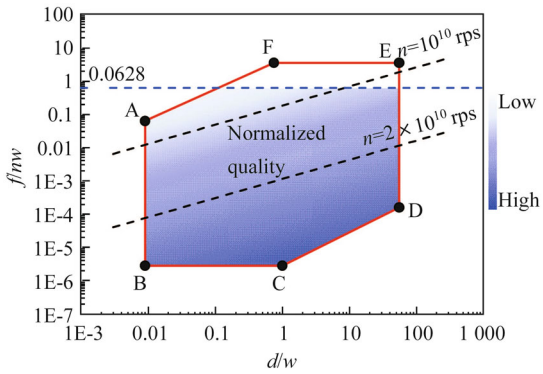

Fig. 17 Predictive machinability for single-grooving

variable regression by the least square criterion in the Matlab. The relation between the absolute average deviation per width of cut (AAd/w) with the normalized machining parameters for both single and multiple grooving were analysed and shown in Table 1. The high coefficients of determination R^2 indicated that all the predictions had a high accuracy. For single grooving, the machining speed $f/(\pi nw)$ and groove dimension d/w factors were identified as governing factors through the calculation of partial eta squared values [45]. Increasing groove dimension d/w could improve groove quality. As for multi-grooving, u/d was revealed as the governing parameter in multi-grooving, and increasing this ratio would improve the multiple groove quality.

4.4 Machinability chart

Due to the fact that some parameters also had critical limits which could not be achieved physically, such as the milling peed. Based on the achievement of the dimensional analysis, the variation of groove quality in terms of AAd with the variation of the depth of cut and feed rate was summarized and shown in Fig. 16, with the simulation results included (black circle). Increasing the depth of cut d and decreasing the feed rate f can improve the groove quality. Due to the restriction of the computational ability, the above machinability chart was limited in dimension. A predictive machining chart was constructed based on some critical parameters and dimensional analysis to qualitatively evaluate the machining performance for a larger scale, as shown in Fig. 17.

The machining chart and predictive machining chart for multi-grooving were also established to provide the guidance for an optimal selection of machining parameters. As shown in Figs. 18 and 19, the normalized qualities below each curve are satisfactory for each cutting speed respectively, and the parameters selected within the zones, which are surrounded by each curve and other boundaries could be used to obtain expected results. It was seen that the area of surrounded zone decreases with the increase of rotational speed. This machining chart could provide all the key constraints and direct guidance for choosing optimal parameters.

The contributions of the work above revealed the mechanism of nano-milling. A more complete understanding of nano-scale processes thus gained can then be used to understand macro-/micro-scale processes through the use of multi-scale mechanics.

The following developments will be useful to the advancement of nano-milling:

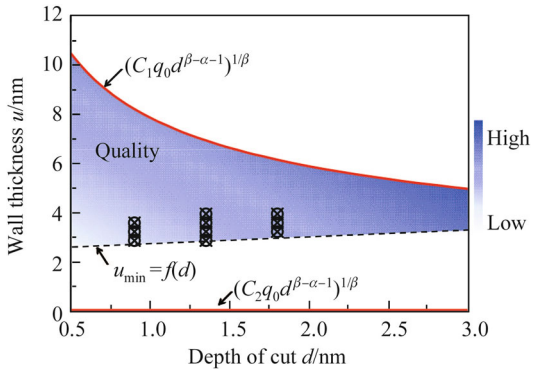

Fig. 18 Machinability chart for multi-grooving

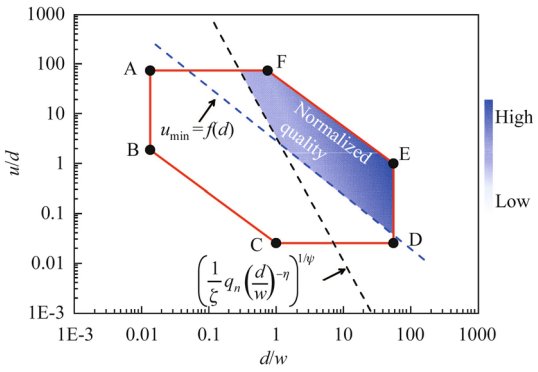

Fig. 19 Predictive machinability chart for multi-grooving

(i) The simulation model can be enlarged to cut more than two grooves with larger depths of cut, thereby obtaining the extreme aspect ratio and an understanding of the underlying physics. These calculations can be made feasible by parallelizing the MD simulation programme.

(ii) Milling tools with complex features (helix or tool angles), which are more akin to the ones used in the macro-scale can be applied. In this way, the effect of the tools on machining can be revealed.

(iii) Experimental work should be performed whenever possible, so that conclusions from MD simulations can be verified. Additionally, the dynamic chip shape variations and its formation process should be captured, which could contribute to a deeper understanding of nano-machining mechanisms.

(iv) More material characters should be included, such as polycrystalline structures and grain boundaries, so that an in-depth understanding of material behaviour in nano-milling can be obtained.

5 Conclusion

This paper has reviewed and discussed the fundamentals of nano-indentation on monocrystalline, polycrystalline and amorphous materials, aiming to understand the nano-deformation mechanisms relevant to nano-machining. Nano-cutting is then reviewed and discussed from the aspects of tool geometry, material properties, machining parameters. Groove profile characteristics fabricated by nano-milling methods and the root cause have also been introduced and discussed with the aid of the study of surface energy, strain rate and residual stresses. It is expected that this paper offers a relatively comprehensive discussion and provides useful information for further investigation into the nano-machining of advanced materials.

Acknowledgment The authors appreciate the Australian Research Council for its financial support to this work. This research was undertaken with the assistance of resources provided at the NCI National Facility systems at the Australian National University and the Intersect Australia Ltd. through the National Computational Merit Allocation Scheme supported by the Australian Government.

References

1. Chae J, Park S, Freiheit T (2006) Investigation of micro-cutting operations. Int J Mach Tools Manuf 46:313–332
2. Malekian M, Park SS, Jun MB (2009) Tool wear monitoring of micro-milling operations. J Mater Process Technol 209:4903–4914
3. Zhang LC, Tanaka H (1999) On the mechanics and physics in the nano-indentation of silicon monocrystals. JSME Int J Ser A Solid Mech Mater Eng 42:546–559
4. Cheong WCD, Zhang LC (2000) Molecular dynamics simulation of phase transformations in silicon monocrystals due to nano-indentation. Nanotechnology 11:173
5. Tang C, Zhang LC (2004) A molecular dynamics analysis of the mechanical effect of water on the deformation of silicon monocrystals subjected to nano-indentation. Nanotechnology 16:15
6. Kim D, Oh S (2006) Atomistic simulation of structural phase transformations in monocrystalline silicon induced by nanoindentation. Nanotechnology 17:2259
7. Minor AM, Asif SS, Shan Z et al (2006) A new view of the onset of plasticity during the nanoindentation of aluminium. Nat Mater 5:697–702
8. Kim KJ, Yoon JH, Cho MH et al (2006) Molecular dynamics simulation of dislocation behavior during nanoindentation on a bicrystal with a $\Sigma = 5$ (210) grain boundary. Mater Lett 60:3367–3372
9. Li J, Guo J, Luo H et al (2016) Study of nanoindentation mechanical response of nanocrystalline structures using molecular dynamics simulations. Appl Surf Sci 364:190–200
10. Szlufarska I, Kalia RK, Nakano A et al (2007) A molecular dynamics study of nanoindentation of amorphous silicon carbide. J Appl Phys 102:23509

11. Qiu C, Zhu P, Fang F et al (2014) Study of nanoindentation behavior of amorphous alloy using molecular dynamics. Appl Surf Sci 305:101–110
12. Bei H, George EP, Hay J et al (2005) Influence of indenter tip geometry on elastic deformation during nanoindentation. Phys Rev Lett 95:045501
13. Shih C, Yang M, Li J (1991) Effect of tip radius on nanoindentation. J Mater Res 6:2623–2628
14. Cheong WCD, Zhang LC, Tanaka H (2001) Some essentials of simulating nano-surfacing processes using the molecular dynamics method. In: Key Engineering Materials, Trans Tech Publ, 2001, pp. 31–42
15. Zhang LC, Cheong WCD (2003) Molecular dynamics simulation of phase transformations in monocrystalline silicon. High Press Surf Sci Eng 57:285
16. Cheong WCD, Zhang LC (2003) Monocrystalline silicon subjected to multi-asperity sliding: nano-wear mechanisms, subsurface damage and effect of asperity interaction. Int J Mater Prod Technol 18:398–407
17. Zhang LC, Johnson K, Cheong WCD (2001) A molecular dynamics study of scale effects on the friction of single-asperity contacts. Tribol Lett 10:23–28
18. Davis JR (1990) Properties and selection: nonferrous alloys and special-purpose materials. ASM Intl 2:1770
19. Pei Q, Lu C, Fang F, Wu H (2006) Nanometric cutting of copper: a molecular dynamics study. Comput Mater Sci 37:434–441
20. Komanduri R, Chandrasekaran N, Raff L (1999) Some aspects of machining with negative-rake tools simulating grinding: a molecular dynamics simulation approach. Philos Mag B 79:955–968
21. Han X (2006) Investigation micro-mechanism of dry polishing using molecular dynamics simulation method. In: 1st IEEE international conference on nano/micro engineered and molecular systems 2006. NEMS'06, pp. 936–941
22. Komanduri R, Chandrasekaran N, Raff L (1998) Effect of tool geometry in nanometric cutting: a molecular dynamics simulation approach. Wear 219:84–97
23. Han X, Lin B, Yu S et al (2002) Investigation of tool geometry in nanometric cutting by molecular dynamics simulation. J Mater Process Technol 129:105–108
24. Komanduri R, Ch and Rasekaran N, Raff L (2001) Molecular dynamics simulation of the nanometric cutting of silicon. Philos Mag B 81:1989–2019
25. Zhao HW, Zhang L, Zhang P et al (2012) Influence of geometry in nanometric cutting single-crystal copper via MD simulation. Adv Mater Res 421:123–128
26. Fang F, Wu H, Zhou W et al (2007) A study on mechanism of nano-cutting single crystal silicon. J Mater Process Technol 184:407–410
27. Zhang LC, Tanaka H (1997) Towards a deeper understanding of wear and friction on the atomic scale—a molecular dynamics analysis. Wear 211:44–53
28. Zhang LC, Tanaka H (1998) Atomic scale deformation in silicon monocrystals induced by two-body and three-body contact sliding. Tribol Int 31:425–433
29. Movahhedy M, Altintas Y, Gadala M (2002) Numerical analysis of metal cutting with chamfered and blunt tools. J Manuf Sci Eng 124:178–188
30. Komanduri R, Chandrasekaran N, Raff L (2000) MD Simulation of nanometric cutting of single crystal aluminum-effect of crystal orientation and direction of cutting. Wear 242:60–88
31. Li J (1961) high-angle tilt boundary—a dislocation core model. J Appl Phys 32:525–541
32. Mylvaganam K, Zhang LC (2010) Effect of nano-scratching direction on the damage in monocrystalline silicon. In: Proceedings of the 6th Australasian congress on applied mechanics, Engineers Australia, p 757
33. Komanduri R, Chandrasekaran N, Raff L (2000) MD simulation of indentation and scratching of single crystal aluminum. Wear 240:113–143
34. Pei Q, Lu C, Lee H (2007) Large scale molecular dynamics study of nanometric machining of copper. Comput Mater Sci 41:177–185
35. Zhu YT, Langdon TG (2005) Influence of grain size on deformation mechanisms: an extension to nanocrystalline materials. Mater Sci Eng A 409:234–242
36. Van Swygenhoven H, Caro A, Farkas D (2001) A molecular dynamics study of polycrystalline FCC metals at the nanoscale: grain boundary structure and its influence on plastic deformation. Mater Sci Eng A 309:440–444
37. Qi Y, Krajewski PE (2007) Molecular dynamics simulations of grain boundary sliding: the effect of stress and boundary misorientation. Acta Mater 55:1555–1563
38. Zhang J, Hartmaier A, Wei Y et al (2013) Mechanisms of anisotropic friction in nanotwinned Cu revealed by atomistic simulations. Model Simul Mater Sci Eng 21:065001
39. Ye Y, Biswas R, Morris J et al (2003) Molecular dynamics simulation of nanoscale machining of copper. Nanotechnology 14:390
40. Fang TH, Weng CI (2000) Three-dimensional molecular dynamics analysis of processing using a pin tool on the atomic scale. Nanotechnology 11:148
41. Zhu PZ, Hu YZ, Ma TB et al (2010) Study of AFM-based nanometric cutting process using molecular dynamics. Appl Surf Sci 256:7160–7165
42. Li J, Liu B, Luo H et al (2016) A molecular dynamics investigation into plastic deformation mechanism of nanocrystalline copper for different nanoscratching rates. Comput Mater Sci 118:66–76
43. Chen J, Liang Y, Chen M et al (2012) Multi-path nanometric cutting of molecular dynamics simulation. J Comput Theor Nanosci 9:1303–1308
44. Oluwajobi A, Chen X (2012) Multi-pass nanometric machining simulation using the molecular dynamics (MD). Key Eng Mater 496:241–246
45. Cui DD, Zhang LC, Mylvaganam K et al (2015) Nano-milling on monocrystalline copper: a molecular dynamics simulation. Mach Sci Technol
46. Cui DD, Mylvaganam K, Zhang LC (2012) Atomic-scale grooving on copper: end-milling versus peripheral-milling. In: Advanced materials research, Trans Tech Publ, pp 546–551
47. Cui DD, Zhang LC, Mylvaganam K (2014) Nano-milling on copper: grooving quality and critical depth of cut. J Comput Theor Nanosci 11:964–970
48. Bao W, Tansel I (2000) Modeling micro-end-milling operations. Part I: analytical cutting force model. Int J Mach Tools Manuf 40:2155–2173
49. Wang Z, Jiao N, Tung S et al (2011) Atomic force microscopy-based repeated machining theory for nanochannels on silicon oxide surfaces. Appl Surf Sci 257:3627–3631
50. Zhang LC, Tanaka H (1999) On the mechanics and physics in the nano-indentation of silicon monocrystals. JSME Int J 42:546–559